

Supersolid devil's staircases of spin-orbit-coupled bosons in optical lattices

Daisuke Yamamoto ^{1,*}, Kotaro Bannai,² Nobuo Furukawa ² and Carlos A. R. Sá de Melo³

¹*Department of Physics, College of Humanities and Sciences, Nihon University, Sakurajosui, Setagaya, Tokyo 156-8550, Japan*

²*Department of Physics and Mathematics, Aoyama Gakuin University, Sagamihara, Kanagawa 252-5258, Japan*

³*School of Physics, Georgia Institute of Technology, Atlanta, Georgia 30332, USA*



(Received 14 January 2022; revised 10 May 2022; accepted 12 July 2022; published 12 August 2022)

We study the emergence of supersolid devil's staircases of spin-orbit-coupled bosons loaded in optical lattices. We consider two- and three-dimensional systems of pseudo-spin-1/2 bosons interacting via local spin-dependent interactions. These interactions together with spin-orbit coupling produce length scales that are commensurate to the lattice spacing. This commensurability leads to devil's staircases of supersolids, with fractal Hausdorff dimensions, which arise from uniform superfluid phases. We show that umklapp processes are essential for the existence of commensurate supersolids, and that without them the devil's staircase does not exist. Lastly, we emphasize the generality of our results, suggest experiments that can unveil these unusual predictions, and discuss potential applications to the case of ⁸⁷Rb.

DOI: [10.1103/PhysRevResearch.4.L032023](https://doi.org/10.1103/PhysRevResearch.4.L032023)

I. INTRODUCTION

For the solid phase of quantum fluids the question “Can solids be superfluids?” has been asked many years ago [1,2] in the context of solid ⁴He, but has so far yielded a negative answer [3–5]. The existence of supersolidity is a very important issue with ramifications in the areas of condensed matter physics (⁴He) [6,7], astrophysics (neutron star cores) [8,9], and ultracold atoms and molecules (large spin atoms, dipolar molecules, and spin-orbit-coupled systems) [10–20]. Some experimental groups have recently reported the existence of supersolids in ultracold dipolar bosons with internal magnetic moments [13,14], following earlier experimental indications of at least metastable supersolidity [10–12]. The supersolid phases were theoretically suggested as a compromise between superfluidity and Wigner crystallization [16], and their stability was confirmed via the inclusion of three-body interactions [21]. While recent experiments [10–14] have stimulated a flurry of theoretical work on supersolid phases of continuum and trapped (harmonic and boxed) dipolar bosons [22–28], experimental investigation of supersolidity in optical lattices is still lacking, albeit the existence of early theoretical work [29–34].

Synthetic spin-orbit coupling (SOC) [17–20,35–37] is another successful tool to realize a coexistent state of superfluid and solid features, in Bose gases with two pseudospin components. Introducing a pair of Raman lasers gives a momentum kick to the two pseudospins in the opposite direction, offering

a one-dimensional (1D) “equal-Rashba-Dresselhaus” (ERD) SOC [35,36]. This creates a superposition of Bose-Einstein condensates (BECs) with two different momenta, producing a density modulation in one direction while keeping the superfluid property [17–19]. This state, called the supersolid stripe, has recently been observed using Bragg reflection [20]. The realization of more general forms of SOC, including two-dimensional (2D) [38–41] and three-dimensional (3D) SOC [42–44], has been an active research topic, mostly with a view to quantum simulations of various topological matters.

Here, we propose the realization of a nontrivial cascade of 2D supersolid phases of pseudospin-1/2 bosons loaded in optical lattices, with the use of ERD SOC, which has now been realized routinely in experiments [35,36]. Our Letter generalizes the case of 1D supersolid stripes studied for weakly interacting bosons either in continuum space [17–20] or in optical lattices [45]. In contrast, we find that devil's staircases of supersolid phases with various 2D crystalline patterns emerge, when the interaction parameters are sufficiently large. Devil's staircases are cascade structures that are commensurate to the underlying lattice and that possess fractal (Hausdorff) dimension deviating substantially from 1.

II. EXPERIMENTAL PROPOSAL

We propose two experimental setups that could be used to create a supersolid devil's staircase of spin-1/2 bosons with SOC in optical lattices. The simplest case is the creation of either a 2D square or a 3D cubic optical lattice with the application of two counterpropagating Raman beams [35] parallel to the optical lattice xy plane, but making angle θ with respect to the x axis. The second experimental setup involves the utilization of radio-frequency chips [37] or monolithic microwave integrated circuits (MMICs) [46], where the axis of the spin-dependent momentum transfer can be changed

*yamamoto.daisuke21@nihon-u.ac.jp

Published by the American Physical Society under the terms of the [Creative Commons Attribution 4.0 International](https://creativecommons.org/licenses/by/4.0/) license. Further distribution of this work must maintain attribution to the author(s) and the published article's title, journal citation, and DOI.

from the x direction, through a relative rotation of the device with respect to the optical lattice.

III. HAMILTONIAN

To investigate the system mentioned above, we consider the Hamiltonian for a 2D square lattice with lattice vectors $\mathbf{a}_1 = (a, 0)$ and $\mathbf{a}_2 = (0, a)$:

$$\hat{\mathcal{H}} = \sum_{(i,j)} (\hat{\mathbf{b}}_i^\dagger \mathcal{T}_{ij} \hat{\mathbf{b}}_j + \text{H.c.}) + \sum_i \hat{\mathbf{b}}_i^\dagger \mathcal{M} \hat{\mathbf{b}}_i + \sum_{is} \frac{U_{ss}}{2} \hat{n}_{is} (\hat{n}_{is} - 1) + U_{\uparrow\downarrow} \sum_i \hat{n}_{i\uparrow} \hat{n}_{i\downarrow}, \quad (1)$$

where $\hat{\mathbf{b}}_i = (\hat{b}_{i\uparrow} \hat{b}_{i\downarrow})^T$ denotes the annihilation operators of bosons with internal state (pseudospin) $s = \uparrow, \downarrow$ at site i , and $\hat{n}_{is} = \hat{b}_{is}^\dagger \hat{b}_{is}$ counts the local number of s bosons. The 2×2 matrices are $\mathcal{T}_{ij} = -t \exp[-i\boldsymbol{\sigma} \cdot \mathbf{k}_T \cdot (\mathbf{r}_i - \mathbf{r}_j)]$ and $\mathcal{M} = -\mu \mathbf{1} + \frac{\hbar\Omega}{2} \boldsymbol{\sigma}_x + \frac{\hbar\delta}{2} \boldsymbol{\sigma}_z$ with $\boldsymbol{\sigma}$ being the Pauli matrices.

We consider the ERD SOC [35,36] with momentum transfer $\mathbf{p}_T = \hbar \mathbf{k}_T = \hbar k_T (\cos \theta \mathbf{e}_x + \sin \theta \mathbf{e}_y)$ along the direction tilted from the lattice x axis by angle θ in the xy plane. Here, \mathbf{e}_x (\mathbf{e}_y) denotes the unit vector in the x (y) direction of the lattice. The Hamiltonian also includes the Rabi coupling Ω and detuning δ , as well as the standard Bose-Hubbard parameters: nearest-neighbor hopping t , chemical potential μ , and intraspin ($s = s'$) and interspin ($s \neq s'$) onsite repulsions $U_{ss'} > 0$ with $U_{\uparrow\downarrow}^2 < U_{\uparrow\uparrow} U_{\downarrow\downarrow}$ to prevent phase separation. We focus on the 2D case, but the 3D case is analogous, in particular, if one uses the same tilt angle θ in the xy plane. We explore the model of Eq. (1) in the regime dominated by t in comparison to $U_{ss'}$.

IV. MULTIPLE CONDENSATES

Diagonalizing the Hamiltonian Eq. (1) with $U_{ss'} = 0$, we obtain the excitation spectra of noninteracting particles:

$$E_{k\pm} = \frac{\epsilon_{k\uparrow} + \epsilon_{k\downarrow}}{2} - \mu \pm \sqrt{\left(\frac{\epsilon_{k\uparrow} - \epsilon_{k\downarrow}}{2}\right)^2 + \left(\frac{\hbar\Omega}{2}\right)^2} \quad (2)$$

with $\epsilon_{ks} = -2t[\cos(k_x a + \tau_s k_T a \cos \theta) + \cos(k_y a + \tau_s k_T a \sin \theta)] + \tau_s \hbar\delta/2$ ($\tau_\uparrow = 1$ and $\tau_\downarrow = -1$). We are interested in the situation where $\hbar|\Omega|/t$ and $\hbar|\delta|/t$ are sufficiently small to create two minima in the lower branch E_{k-} within the first Brillouin zone (BZ). For instance, this is achieved for $\hbar|\Omega|/t < 4 \sum_{j=1,2} |\sin \mathbf{k}_T \cdot \mathbf{a}_j \tan \mathbf{k}_T \cdot \mathbf{a}_j|$, when $\delta = 0$. In this case, when the temperature is sufficiently low, the particles form BECs with wave vectors at the two minima of E_{k-} , say, \mathbf{k}_1 and \mathbf{k}_2 . However, in the presence of interactions $U_{ss'}$, the momenta where condensation occurs are modified to $\tilde{\mathbf{k}}_1$ and $\tilde{\mathbf{k}}_2$. These momenta can be parametrized as $\tilde{\mathbf{k}}_1 = -\tilde{\mathbf{q}} + \delta\mathbf{q}$ and $\tilde{\mathbf{k}}_2 = \tilde{\mathbf{q}} + \delta\mathbf{q}$. The deviation $\delta\mathbf{q}$ reflects the parity asymmetry caused by nonzero detuning δ and/or by broken Z_2 -symmetry interactions $U_{\uparrow\uparrow} \neq U_{\downarrow\downarrow}$.

When BECs are formed at $\tilde{\mathbf{k}}_1$ and $\tilde{\mathbf{k}}_2$, the interference of the two produces higher harmonics with wave vectors differing by an integer multiple of $2\tilde{\mathbf{q}}$. This indicates that the expectation

value of $\langle \hat{b}_{is} \rangle$ acquires a spatial modulation of the form

$$\langle \hat{b}_{is} \rangle = \Psi_{is} = \sqrt{\rho} \sum_n \psi_{ns} e^{i\mathbf{q}_n \cdot \mathbf{r}_i} \quad (3)$$

with $\mathbf{q}_n = (2n-1)\tilde{\mathbf{q}} + \delta\mathbf{q}$ ($n \in \mathbb{Z}$). Here, $\rho = \sum_{is} |\Psi_{is}|^2 / M$ is the particle filling per site, where M is the number of lattice sites. The Fourier amplitudes ψ_{ns} represent BEC order parameters at each momentum \mathbf{q}_n and are normalized such that $\sum_{ns} |\psi_{ns}|^2 = 1$.

The subscript n labels the harmonic components (HCs); for example, $n = 0, 1$ correspond to the two fundamental matter waves with wave vectors $\mp\tilde{\mathbf{q}} + \delta\mathbf{q}$, and $n = -1, 2$ are the second harmonics with $\mp 3\tilde{\mathbf{q}} + \delta\mathbf{q}$, and so on.

Using Eq. (3), we minimize the variational energy per particle

$$\frac{E_0}{M\rho} = \sum_n (\psi_{n\uparrow}^* \quad \psi_{n\downarrow}^*) \begin{pmatrix} \epsilon_{\mathbf{q}_n\uparrow} - \mu & \hbar\Omega/2 \\ \hbar\Omega/2 & \epsilon_{\mathbf{q}_n\downarrow} - \mu \end{pmatrix} \begin{pmatrix} \psi_{n\uparrow} \\ \psi_{n\downarrow} \end{pmatrix} + \sum_{n_1+n_2=n_3+n_4} \sum_{ss'} \frac{U_{ss'}\rho}{2} \psi_{n_1s}^* \psi_{n_2s'}^* \psi_{n_3s} \psi_{n_4s}, \quad (4)$$

with respect to the order parameters ψ_{ns} and the wave vectors $\tilde{\mathbf{q}}$ and $\delta\mathbf{q}$ under the condition $\sum_{ns} |\psi_{ns}|^2 = 1$. The sum in the interaction term is over all possible subsets of the HC's that satisfy momentum conservation implying the restriction $n_1 + n_2 = n_3 + n_4$. When $2\tilde{\mathbf{q}}$ is commensurate to the lattice spacing, we also need to consider umklapp scattering processes with momentum conservation modulo the reciprocal lattice vectors $\mathbf{G}_1 = (2\pi/a, 0)$ and $\mathbf{G}_2 = (0, 2\pi/a)$, as we shall explain later. We have verified that a numerical minimization of the real-space Gross-Pitaevskii energy functional [47] for Ψ_{is} in its most general form yields the same results as those under the ansatz Eq. (3) in all the examples investigated.

In Fig. 1(b), we show the ground-state distribution of the order parameter amplitude $|\psi_{ns}|$, in the first BZ, for parameters given in the caption. Remarkably, we find that the $(\tilde{q}_x, \tilde{q}_y)$ components of $\tilde{\mathbf{q}}$, in units of π/a , may be rational numbers even when the SOC momentum components (k_{Tx}, k_{Ty}) , in units of π/a , are irrational numbers, while the components of $\delta\mathbf{q}$ can have any real value. For the parameters of Fig. 1(b), where $\delta = 0$ and $U_{\uparrow\uparrow} = U_{\downarrow\downarrow}$, then $\delta\mathbf{q} = \mathbf{0}$, and the fundamental BEC wave vectors are $\pm\tilde{\mathbf{q}} = \pm(1/2, 1/4)\pi/a$.

When \tilde{q}_x and \tilde{q}_y are commensurate with π/a , the number of the HC's is finite. For example, in Fig. 1(b), the wave vectors of second-harmonic components are given as $\mathbf{q}_{-1,2} = \pm 3\tilde{\mathbf{q}} = \pm(3/2, 3/4)\pi/a$, which are equivalent to $\pm(-1/2, 3/4)\pi/a$ in the first BZ. In this case, third and higher harmonics are reduced to either the fundamental or the second harmonic wave vectors due to momentum-space periodicity, and thus it is sufficient to consider up to the second components. For a general commensurate wave vector $\tilde{\mathbf{q}} = (\xi_1/\eta_1, \xi_2/\eta_2)\pi/a$, with relatively prime integers ξ_ℓ and η_ℓ , the number of independent HC's is given by $N_{\text{HC}} = \text{LCM}[\eta_1, \eta_2]$, where LCM means least common multiple. The interference of BECs with N_{HC} components produces the spatial modulation with the wave vectors $\mathbf{Q} = \pm 2\tilde{\mathbf{q}} = \pm[(\xi_1/\eta_1)\mathbf{G}_1 + (\xi_2/\eta_2)\mathbf{G}_2]$, showing a modulation period $\Lambda_x = \eta_1 a$ and $\Lambda_y = \eta_2 a$ in the density

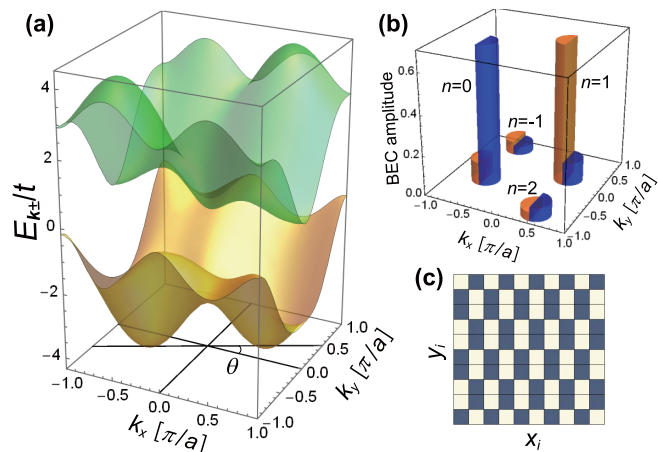


FIG. 1. (a) Excitation spectra of noninteracting particles $E_{k_{\pm}}$ measured from μ and (b) the distributions of the BEC components for $\hbar\Omega = 3t$, $k_T = 0.57\pi/a$, $\theta = 0.15\pi$, $\delta = 0$, $U_{\uparrow\uparrow} = U_{\downarrow\downarrow} = U = 10t/\rho$, and $U_{\uparrow\downarrow} = 0.9U$. The blue and orange bars in (b) represent the BEC amplitude $|\psi_{n,s}|$ for $s = \uparrow$ and $s = \downarrow$, respectively. (c) Lattice superstructure of the particle density $\sum_s |\Psi_{is}|^2$, resulting from the multiple BECs of (b), in the real space. The density modulation is $\approx \pm 7.1\%$ of the average filling factor $\rho \gg 1$ for the lattice sites with the lighter and darker colors, respectively.

profile $\sum_s |\Psi_{is}|^2$, as seen in Fig. 1(c), where $\eta_1 = 2$ and $\eta_2 = 4$.

V. COMMENSURABILITY AND UMKLAPP SCATTERING

Next, we show that the difference vector $2\bar{q}$ between the two fundamental matter waves $\mathbf{q}_{0,1} = \pm\bar{q} + \delta\mathbf{q}$ must always be of the form $\frac{\xi_1}{\eta_1}\mathbf{G}_1 + \frac{\xi_2}{\eta_2}\mathbf{G}_2$ in the ground state, as seen from the conditions satisfied by the phases ϕ_{ns} of the order parameters $\psi_{ns} = |\psi_{ns}|e^{i\phi_{ns}}$ for the minimization of the ground-state energy in Eq. (4). First, from the spin-flip terms in Eq. (4), the relative phase between $\psi_{n\uparrow}$ and $\psi_{n\downarrow}$ with the same n is determined by the sign of Ω to be $\phi_{n\uparrow} - \phi_{n\downarrow} = \pi$ ($\phi_{n\uparrow} - \phi_{n\downarrow} = 0$) when $\Omega > 0$ ($\Omega < 0$). Second, given the previous condition, the interaction terms involving both intraspin U_{ss} and interspin $U_{ss'}$ (with $s \neq s'$) interactions produce the factor

$$\mathcal{A}_{ss'} \cos[\phi_{n_1s} + \phi_{n_2s} - \phi_{n_3s} - \phi_{n_4s}], \quad (5)$$

with positive interaction coefficients ($\mathcal{A}_{ss'} > 0$). Here, we choose the global phase to be $\phi_{0\uparrow} = -\phi_{1\uparrow} = -\bar{\phi}/2$, without loss of generality. The second harmonic components $n = 2$ and -1 arise from the scattering processes of the type $(n_1, n_2; n_3, n_4) = (2, 0; 1, 1)$ and $(-1, 1; 0, 0)$, respectively. Thus, their phases must be $\phi_{2\uparrow} = 3\bar{\phi}/2 + \pi$ and $\phi_{-1\uparrow} = -3\bar{\phi}/2 + \pi$ to minimize the interaction energy in Eq. (5). Analogously, the momentum conservation $n_1 + n_2 = n_3 + n_4$ and the minimization of the interaction energy lead to the conclusion that the up-spin phases of the HCs satisfy

$$\phi_{n\uparrow} = \frac{2n-1}{2}\bar{\phi} + \arccos[(-1)^{\frac{|2n-1|-1}{2}}] \quad (6)$$

with $n \in \mathbb{Z}$, while the down-spin phases are $\phi_{n\downarrow} = \phi_{n\uparrow} - \pi$ for $\Omega > 0$ or $\phi_{n\downarrow} = \phi_{n\uparrow}$ for $\Omega < 0$. The last degree of freedom

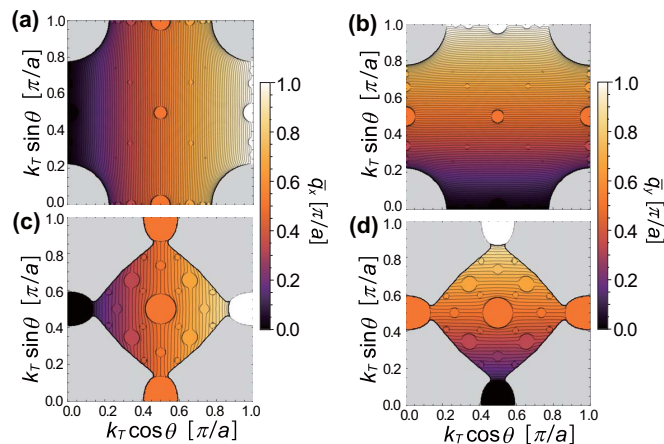


FIG. 2. Contour plots of the values of \bar{q}_x and \bar{q}_y in the $k_T \cos \theta$ vs $k_T \sin \theta$ plane for (a, b) $\hbar\Omega = 1.2t$ and (c, d) $\hbar\Omega = 3t$ ($\delta = 0$, $U_{\uparrow\uparrow} = U_{\downarrow\downarrow} = U = 8t/\rho$, and $U_{\uparrow\downarrow} = 0.9U$ for both). The gray areas represent the regions where a single-BEC superfluid is the ground state.

is the relative phase $\bar{\phi}$ between the two fundamental BECs, discussed next.

When the difference vector between the two fundamental matter waves is commensurate to the lattice spacing, that is, $2\bar{q} = \frac{\xi_1}{\eta_1}\mathbf{G}_1 + \frac{\xi_2}{\eta_2}\mathbf{G}_2$, umklapp scattering processes with the total momentum transfer equal to reciprocal lattice vectors $n_1 + n_2 - n_3 - n_4 = \pm \text{LCM}[\eta_1, \eta_2] = \pm N_{\text{HC}}$ must be considered in the second sum of Eq. (4). Using Eqs. (5) and (6), it is easy to see that the sum of the umklapp scattering terms takes the form

$$\mathcal{B} \cos[\Theta] \text{ with } \Theta = N_{\text{HC}}\bar{\phi}, \quad (7)$$

which is analogous to the Josephson energy between two superconductors: when \mathcal{B} is negative (positive) then the energy takes its minimum $-|\mathcal{B}|$ for $\Theta = 0$ ($\Theta = \pi$) mod 2π . Thus, the existence of the umklapp scattering can always reduce the total energy. This also implies that the commensurate supersolid state breaks Z_N symmetry (with $N = N_{\text{HC}}$) with respect to the choice of $\bar{\phi}$, in addition to the breaking of $U(1)$ symmetry associated with the global phase fixed earlier.

VI. SUPERSOLID DEVIL'S STAIRCASE

As discussed above, commensurate ground states with rational values of \bar{q}_x and \bar{q}_y (in units of π/a) are always favored against incommensurate ones. This indicates that \bar{q}_x and \bar{q}_y develop plateaus at rational values for numerous intervals of input variables k_{T_x} and k_{T_y} , thus forming a devil's staircase structure with an infinite number of steps. In Fig. 2, we show the values of \bar{q}_x and \bar{q}_y as functions of $k_{T_x} = k_T \cos \theta$ and $k_{T_y} = k_T \sin \theta$ for two example sets of parameters. We show only the first quadrant of the first BZ since the function \bar{q}_x (\bar{q}_y) is odd in k_{T_x} (k_{T_y}) and even in k_{T_y} (k_{T_x}).

In Fig. 3, we show examples of \bar{q}_x versus k_T in the limit of 1D supersolid stripes to explain the fractal nature. A box-counting analysis for the plateau width is shown in Fig. 3(b). The function $L(\epsilon)$ is the difference between the total width of the staircase and the sum of the plateau widths larger than

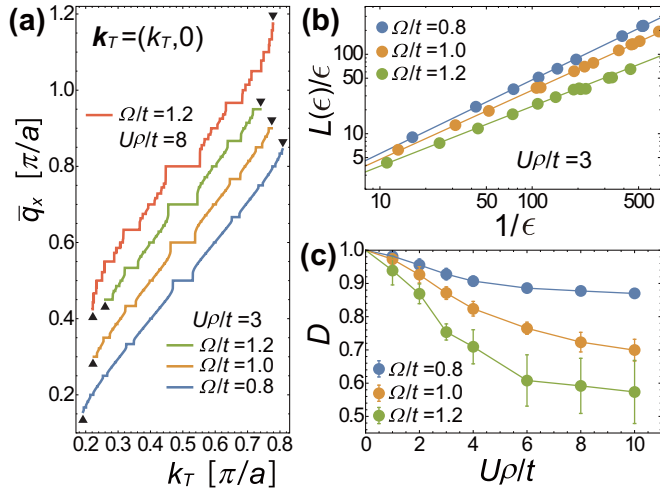


FIG. 3. (a) Supersolid devil's staircases for \bar{q}_x vs k_T at SOC angle $\theta = 0$. The orange, green, and red lines are vertically shifted by 0.1, 0.2, and 0.3 with respect to the blue line to avoid overlap. The black triangles at the end points indicate the emergence of single-BEC superfluid phases. (b) Plots of the function $L(\epsilon)/\epsilon$ vs $1/\epsilon$ characterizing the plateau widths ϵ of the devil's staircases. (c) Hausdorff fractal dimension D as a function of $U\rho/t$. We set $U_{\uparrow\uparrow} = U_{\downarrow\downarrow} = U$, $U_{\uparrow\downarrow} = 0.9U$, and $\delta = 0$ for all panels.

$\epsilon > 0$. The slope of the log-log plot of $L(\epsilon)/\epsilon$ versus $1/\epsilon$ in the limit of $\epsilon \rightarrow 0$ gives the Hausdorff fractal dimension D of the system [48]. If $D < 1$, the incommensurate phases form a fractal set of measure zero, meaning that we have a complete devil's staircase of commensurate (supersolid) phases. In Fig. 3(c), we show D versus $U\rho/t$ to indicate the fractality of the staircase. Notice that when interactions tend to zero ($U\rho/t \rightarrow 0$) then the Hausdorff dimension $D \rightarrow 1$, and there is no devil's staircase. This reinforces that interactions are essential for the emergence of the supersolid devil's staircase, which in practice is not observable for small $U\rho/t$ [45].

For fixed t , $U_{ss'}$, Ω , and δ , it is easier to vary the tilt angle θ , as changing k_T requires a different laser wavelength for the Raman setup, or a different radio-frequency (microwave) wavelength in the atom-chip (MMIC) configuration.

Thus, in Fig. 4, we show examples of \bar{q}_x and \bar{q}_y for fixed k_T and changing θ . In Fig. 4(a), $k_T = 2.02\pi/a$, but the vector \mathbf{k}_T is closer to pointing along the k_x direction since $73.5^\circ < \theta < 84.5^\circ$ [see Fig. 4(c)]. In this case, the value of \bar{q}_y is nearly (or exactly) zero, while \bar{q}_x take fractional values with the largest steps being at $\bar{q}_x = \{1/2, 1/3, 1/4, 1/5\}\pi/a$. These are supersolid stripes, where the density $\sum_s |\Psi_{is}|^2$ is uniform along the y direction and modulated along the x direction with period $\{2, 3, 4, 5\}a$. In Fig. 4(b), $k_T = 0.72\pi/a$, but the vector \mathbf{k}_T is closer to the diagonal in the first quadrant of the first BZ [see Fig. 4(d)]. In this case, we have a cascade of supersolid phases with 2D crystalline patterns; the most prominent ones have the largest ladder steps characterized by the ordered pairs $(\bar{q}_x, \bar{q}_y) = \{(1/3, 2/3); (2/5, 3/5); (1/2, 1/2); (2/3, 1/3); (3/5, 2/5)\}$ in units of π/a . The box-counting analysis gives the Hausdorff dimension $D = 0.55(3)$ in this case.

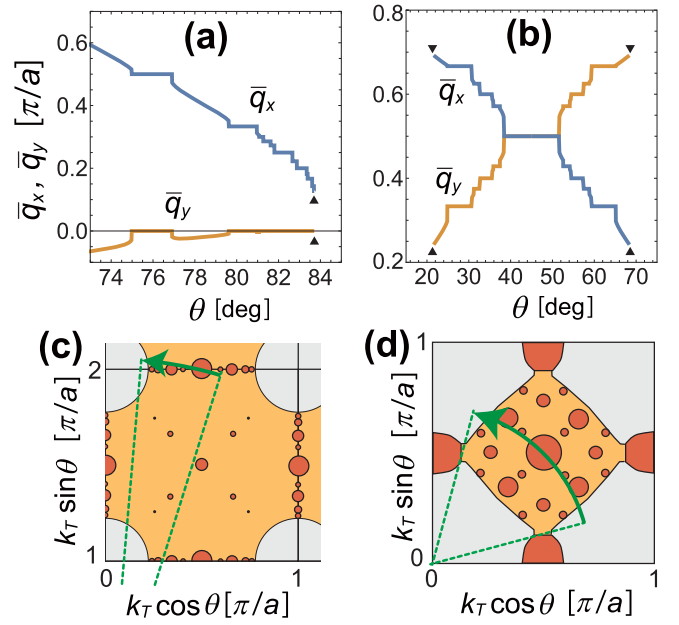


FIG. 4. Supersolid devil's staircases for \bar{q}_x and \bar{q}_y vs SOC angle θ for fixed values of k_T . Panel (a) [(b)] has the same parameters as in Figs. 2(a) and 2(b) [Figs. 2(c) and 2(d)] along the arc with $k_T = 2.02\pi/a$ [$k_T = 0.72\pi/a$], indicated by the arrow in (c) [(d)]. The triangles have the same meaning as in Fig. 3(a).

VII. EXPERIMENTAL DETECTION

The simplest experiments to detect supersolid phases and their staircase structure are momentum-space measurements. Both the momentum distribution $n(\mathbf{k})$ in time of flight [49] and the structure factor $S(\mathbf{q})$ obtained from Bragg spectroscopy [50] can reveal the fundamental and higher-order momentum components of the order parameter density. In addition, the real-space periodic modulations of the supersolids can be detected, in principle, using quantum gas microscopes [51–53] or magnifiers [54].

When atoms have anisotropic interactions $U_{\uparrow\uparrow} \neq U_{\downarrow\downarrow}$, then Z_2 symmetry is broken. This is the case for two hyperfine states of ^{87}Rb atoms, $|\uparrow\rangle = |F=1, m_F=0\rangle$ and $|\downarrow\rangle = |F=1, m_F=-1\rangle$, where $U_{\downarrow\downarrow} \approx U_{\uparrow\uparrow} \approx 0.995U_{\uparrow\uparrow}$ [35,55]. The broken spin symmetry can be compensated by the detuning $\delta = \delta_0 = -\rho(U_{\uparrow\uparrow} - U_{\downarrow\downarrow})/2$, since the anisotropy is small ($|U_{\uparrow\uparrow} - U_{\downarrow\downarrow}| \ll \sum_{ss'} U_{ss'}$) [18]. In this case, the shift $\delta\mathbf{q}$ of the BEC momenta is negligible and the results for $U_{\uparrow\uparrow} \neq U_{\downarrow\downarrow}$ with $\delta = \delta_0$ are essentially identical to the results for $U_{\uparrow\uparrow} \rightarrow \bar{U}$, $U_{\downarrow\downarrow} \rightarrow \bar{U}$, and $\delta_0 \rightarrow 0$, where $\bar{U} = (U_{\uparrow\uparrow} + U_{\downarrow\downarrow})/2$.

VIII. CONCLUSIONS

We have investigated the existence of supersolid devil's staircases for spin-orbit-coupled bosons in optical lattices, proposed experimental setups, and suggested detection techniques for their direct observation. Furthermore, we showed that the cascade of supersolid phases with various 2D (or 1D) crystalline patterns occurs due to the stabilization mechanism by umklapp scattering. We emphasize that our umklapp mechanism for forming devil's staircases with local interactions is

sharply distinct from that in dipolar gases with long-ranged interactions [32]. This Letter opens the door for studying supersolid devil's staircases in spin-orbit-coupled atoms, and, more generally, provides a fundamental idea for understanding the commensuration of ordering vectors with possible applications to Fulde-Ferrell-Larkin-Ovchinnikov superconductivity [56] and chiral magnets [57].

ACKNOWLEDGMENTS

D.Y. was supported by Japan Society for the Promotion of Science (JSPS) KAKENHI Grants No. 18K03525 and No. 21H05185, Japan Science and Technology Agency (JST) CREST Grant No. JPMJCR1673, and JST PRESTO Grant No. JPMJPR2118. D.Y. and N.F. were supported by JSPS KAKENHI Grant No. 22H01171.

-
- [1] A. J. Leggett, Can a Solid Be “Superfluid”?, *Phys. Rev. Lett.* **25**, 1543 (1970).
- [2] G. V. Chester, Speculations on Bose-Einstein condensation and quantum crystals, *Phys. Rev. A* **2**, 256 (1970).
- [3] D. Y. Kim and M. H. W. Chan, Absence of Supersolidity in Solid Helium in Porous Vycor Glass, *Phys. Rev. Lett.* **109**, 155301 (2012).
- [4] M. H. W. Chan, R. Hallock, and L. Reatto, Overview on solid ^4He and the issue of supersolidity, *J. Low Temp. Phys.* **172**, 317 (2013).
- [5] A. Eyal, X. Mi, A. V. Talanov, and J. D. Reppy, Multiple mode torsional oscillator studies and evidence for supersolidity in bulk ^4He , *Proc. Natl. Acad. Sci. USA* **113**, E3203 (2016).
- [6] J. Day and J. Beamish, Low-temperature shear modulus changes in solid ^4He and connection to supersolidity, *Nature (London)* **450**, 853 (2007).
- [7] H. J. Maris, Effect of elasticity on torsional oscillator experiments probing the possible supersolidity of Helium, *Phys. Rev. B* **86**, 020502(R) (2012).
- [8] K. Rajagopal and R. Sharma, Crystallography of three-flavor quark matter, *Phys. Rev. D* **74**, 094019 (2006).
- [9] B. Haskell, N. Andersson, D. I. Jones, and L. Samuelsson, Are Neutron Stars with Crystalline Color-Superconducting Cores Relevant for the LIGO Experiment?, *Phys. Rev. Lett.* **99**, 231101 (2007).
- [10] F. Böttcher, J. N. Schmidt, M. Wenzel, J. Hertkorn, M. Guo, T. Langen, and T. Pfau, Transient Supersolid Properties in an Array of Dipolar Quantum Droplets, *Phys. Rev. X* **9**, 011051 (2019).
- [11] L. Tanzi, E. Lucioni, F. Famà, J. Catani, A. Fioretti, C. Gabbanini, R. N. Bisset, L. Santos, and G. Modugno, Observation of a Dipolar Quantum Gas with Metastable Supersolid Properties, *Phys. Rev. Lett.* **122**, 130405 (2019).
- [12] L. Chomaz, D. Petter, P. Ilzhöfer, G. Natale, A. Trautmann, C. Politi, G. Durastante, R. M. W. van Bijnen, A. Patscheider, M. Sohmen, M. J. Mark, and F. Ferlaino, Long-Lived and Transient Supersolid Behaviors in Dipolar Quantum Gases, *Phys. Rev. X* **9**, 021012 (2019).
- [13] M. A. Norcia, C. Politi, L. Klaus, E. Poli, M. Sohmen, M. J. Mark, R. Bisset, L. Santos, and F. Ferlaino, Two-dimensional supersolidity in a dipolar quantum gas, *Nature (London)* **596**, 357 (2021).
- [14] L. Tanzi, J. G. Maloberti, G. Biagioni, A. Fioretti, C. Gabbanini, and G. Modugno, Evidence of superfluidity in a dipolar supersolid from non-classical rotational inertia, *Science* **371**, 1162 (2021).
- [15] K. Góral, L. Santos, and M. Lewenstein, Quantum Phases of Dipolar Bosons in Optical Lattices, *Phys. Rev. Lett.* **88**, 170406 (2002).
- [16] K. Mitra, C. J. Williams, and C. A. R. Sá de Melo, Hexatic, Wigner crystal, and superfluid phases of dipolar bosons, [arXiv:0903.4655v1](https://arxiv.org/abs/0903.4655v1).
- [17] T. L. Ho and S. Zhang, Bose-Einstein Condensates with Spin-Orbit Interaction, *Phys. Rev. Lett.* **107**, 150403 (2011).
- [18] Y. Li, L. P. Pitaevskii, and S. Stringari, Quantum Tricriticality and Phase Transitions in Spin-Orbit Coupled Bose-Einstein Condensates, *Phys. Rev. Lett.* **108**, 225301 (2012).
- [19] Y. Li, G. I. Martone, L. P. Pitaevskii, and S. Stringari, Superstripes and the Excitation Spectrum of a Spin-Orbit-Coupled Bose-Einstein Condensate, *Phys. Rev. Lett.* **110**, 235302 (2013).
- [20] J. R. Li, J. Lee, W. Huang, S. Burchesky, B. Shteynas, F. C. Top, A. O. Jamison, and W. Ketterle, A stripe phase with supersolid properties in spin-orbit-coupled Bose-Einstein condensates, *Nature (London)* **543**, 91 (2017).
- [21] Z.-K. Lu, Y. Li, D. S. Petrov, and G. V. Shlyapnikov, Stable Dilute Supersolid of Two-Dimensional Dipolar Bosons, *Phys. Rev. Lett.* **115**, 075303 (2015).
- [22] Y. C. Zhang, F. Maucher, and T. Pohl, Supersolidity around a Critical Point in Dipolar Bose-Einstein Condensates, *Phys. Rev. Lett.* **123**, 015301 (2019).
- [23] P. B. Blakie, D. Baillie, L. Chomaz, and F. Ferlaino, Supersolidity in an elongated dipolar condensate, *Phys. Rev. Research* **2**, 043318 (2020).
- [24] A. Gallemí, S. M. Roccuzzo, S. Stringari, and A. Recati, Quantized vortices in dipolar supersolid Bose-Einstein-condensed gases, *Phys. Rev. A* **102**, 023322 (2020).
- [25] S. M. Roccuzzo, A. Gallemí, A. Recati, and S. Stringari, Rotating a Supersolid Dipolar Gas, *Phys. Rev. Lett.* **124**, 045702 (2020).
- [26] F. Ancilotto, M. Barranco, M. Pi, and L. Reatto, Vortex properties in the extended supersolid phase of dipolar Bose-Einstein condensates, *Phys. Rev. A* **103**, 033314 (2021).
- [27] J. Hertkorn, J. N. Schmidt, M. Guo, F. Böttcher, K. S. H. Ng, S. D. Graham, P. Uerlings, H. P. Büchler, T. Langen, M. Zwerlein, and T. Pfau, Supersolidity in Two-Dimensional Trapped Dipolar Droplet Arrays, *Phys. Rev. Lett.* **127**, 155301 (2021).
- [28] J. Hertkorn, J. N. Schmidt, M. Guo, F. Böttcher, K. S. H. Ng, S. D. Graham, P. Uerlings, T. Langen, M. Zwerlein, and T. Pfau, Pattern formation in quantum ferrofluids: from supersolids to superglasses, *Phys. Rev. Research* **3**, 033125 (2021).
- [29] C. Menotti, C. Trefzger, and M. Lewenstein, Metastable States of a Gas of Dipolar Bosons in a 2D Optical Lattice, *Phys. Rev. Lett.* **98**, 235301 (2007).
- [30] S. Yi, T. Li, and C. P. Sun, Novel Quantum Phases of Dipolar Bose Gases in Optical Lattices, *Phys. Rev. Lett.* **98**, 260405 (2007).

- [31] I. Danshita and C. A. R. Sá de Melo, Stability of Superfluid and Supersolid Phases of Dipolar Bosons in Optical Lattices, *Phys. Rev. Lett.* **103**, 225301 (2009).
- [32] B. Capogrosso-Sansone, C. Trefzger, M. Lewenstein, P. Zoller, and G. Pupillo, Quantum Phases of Cold Polar Molecules in 2D Optical Lattices, *Phys. Rev. Lett.* **104**, 125301 (2010).
- [33] L. Pollet, J. D. Picon, H. P. Büchler, and M. Troyer, Supersolid Phase with Cold Polar Molecules on a Triangular Lattice, *Phys. Rev. Lett.* **104**, 125302 (2010).
- [34] D. Yamamoto, I. Danshita, and C. A. R. Sá de Melo, Dipolar bosons in triangular optical lattices: Quantum phase transitions and anomalous hysteresis, *Phys. Rev. A* **85**, 021601(R) (2012).
- [35] Y. J. Lin, K. Jiménez-García, and I. B. Spielman, Spin-orbit-coupled Bose-Einstein condensates, *Nature (London)* **471**, 83 (2011).
- [36] J.-Y. Zhang, S.-C. Ji, Z. Chen, L. Zhang, Z.-D. Du, B. Yan, G.-S. Pan, B. Zhao, Y.-J. Deng, H. Zhai, S. Chen, and J.-W. Pan, Collective Dipole Oscillations of a Spin-Orbit Coupled Bose-Einstein Condensate, *Phys. Rev. Lett.* **109**, 115301 (2012).
- [37] B. M. Anderson, I. B. Spielman, and G. Juzeliūnas, Magnetically Generated Spin-Orbit Coupling for Ultracold Atoms, *Phys. Rev. Lett.* **111**, 125301 (2013).
- [38] L. Huang, Z. Meng, P. Wang, P. Peng, S.-L. Zhang, L. Chen, D. Li, Q. Zhou, and J. Zhang, Experimental realization of two-dimensional synthetic spin-orbit coupling in ultracold Fermi gases, *Nat. Phys.* **12**, 540 (2016).
- [39] J.-S. Pan, W. Zhang, W. Yi, and G.-C. Guo, Bose-Einstein condensate in an optical lattice with Raman-assisted two-dimensional spin-orbit coupling, *Phys. Rev. A* **94**, 043619 (2016).
- [40] B. Z. Wang, Y.-H. Lu, W. Sun, S. Chen, Y. Deng, and X.-J. Liu, Dirac-, Rashba-, and Weyl-type spin-orbit couplings: Toward experimental realization in ultracold atoms, *Phys. Rev. A* **97**, 011605(R) (2018).
- [41] W. Sun, B.-Z. Wang, X.-T. Xu, C.-R. Yi, L. Zhang, Z. Wu, Y. Deng, X.-J. Liu, S. Chen, and J.-W. Pan, Highly Controllable and Robust 2D Spin-Orbit Coupling for Quantum Gases, *Phys. Rev. Lett.* **121**, 150401 (2018).
- [42] B. M. Anderson, G. Juzeliūnas, V. M. Galitski, and I. B. Spielman, Synthetic 3D Spin-Orbit Coupling, *Phys. Rev. Lett.* **108**, 235301 (2012).
- [43] Y.-H. Lu, B.-Z. Wang, and X.-J. Liu, Ideal Weyl semimetal with 3D spin-orbit coupled ultracold quantum gas, *Sci. Bull.* **65**, 2080 (2020).
- [44] Z.-Y. Wang, X.-C. Cheng, B.-Z. Wang, J.-Y. Zhang, Y.-H. Lu, C.-R. Yi, S. Niu, Y. Deng, X.-J. Liu, S. Chen, and J.-W. Pan, Realization of an ideal Weyl semimetal band in a quantum gas with 3D spin-orbit coupling, *Science* **372**, 271 (2021).
- [45] D. Yamamoto, I. B. Spielman, and C. A. R. Sá de Melo, Quantum Phases of Two-Component Bosons with Spin-Orbit Coupling in Optical Lattices, *Phys. Rev. A* **96**, 061603(R) (2017).
- [46] D. Lao, C. Raman and C. A. R. Sá de Melo, Nematic-Orbit Coupling and Nematic Density Waves in Spin-1 Condensates, *Phys. Rev. Lett.* **124**, 173203 (2020).
- [47] M. Killi, S. Trotzky, and A. Paramekanti, Anisotropic quantum quench in the presence of frustration or background gauge fields: A probe of bulk currents and topological chiral edge modes, *Phys. Rev. A* **86**, 063632 (2012).
- [48] E. S. Nascimento, J. P. de Lima, and S. R. Salina, Modulated phases and Devil's staircases in a layered mean-field version of the ANNNI model, *Physica A* **409**, 78 (2014).
- [49] M. Greiner, O. Mandel, T. Esslinger, T. W. Hänsch, and I. Bloch, Quantum phase transition from a superfluid to a Mott insulator in a gas of ultracold atoms, *Nature (London)* **415**, 39 (2002).
- [50] T. A. Corcovilos, S. K. Baur, J. M. Hitchcock, E. J. Mueller, and R. G. Hulet, Detecting antiferromagnetism of atoms in an optical lattice via optical Bragg scattering, *Phys. Rev. A* **81**, 013415 (2010).
- [51] W. S. Bakr, J. Gillen, A. Peng, S. Fölling, and M. Greiner, A quantum gas microscope for detecting single atoms in a Hubbard regime optical lattice, *Nature (London)* **462**, 74 (2009).
- [52] M. Boll, T. A. Hilker, G. Salomon, A. Omran, J. Nespolo, L. Pollet, I. Bloch, and C. Gross, Spin- and density-resolved microscopy of antiferromagnetic correlations in Fermi-Hubbard chains, *Science* **353**, 1257 (2016).
- [53] D. Mitra, P. Brown, E. Guardado-Sanchez, S. Kondov, T. Devakul, D. Huse, P. Schauss, and W. Bakr, Quantum gas microscopy of an attractive Fermi-Hubbard system, *Nat. Phys.* **14**, 173 (2018).
- [54] L. Asteria, H. P. Zahn, M. N. Kosch, K. Sengstock, and C. Weitenberg, Quantum gas magnifier for sub-lattice-resolved imaging of three-dimensional quantum systems, *Nature (London)* **599**, 571 (2021).
- [55] A. Widera, F. Gerbier, S. Fölling, T. Gericke, O. Mandel, and I. Bloch, Precision measurement of spin-dependent interaction strengths for spin-1 and spin-2 ^{87}Rb atoms, *New J. Phys.* **8**, 152 (2006).
- [56] J. J. Kinnunen, J. E. Baarsma, J.-P. Martikainen, and P. Törmä, The Fulde-Ferrell-Larkin-Ovchinnikov state for ultracold fermions in lattice and harmonic potentials: A review, *Rep. Prog. Phys.* **81**, 046401 (2018).
- [57] K. Tsuruta, M. Mito, Y. Kousaka, J. Akimitsu, J. Kishine, Y. Togawa, H. Ohsumi, and K. Inoue, Discrete change in magnetization by chiral soliton lattice formation in the chiral magnet $\text{Cr}_{1/3}\text{NbS}_2$, *J. Phys. Soc. Jpn.* **85**, 013707 (2016).